CrystEngComm

RSC Publishing

COMMUNICATION

View Article Online
View Journal | View Issue

Cite this: *CrystEngComm*, 2013, **15**, 9394

Received 16th August 2013,
Accepted 8th October 2013

DOI: 10.1039/c3ce41632a

www.rsc.org/crystengcomm

Syntheses of two imidazolate-4-amide-5-imidate linker-based hexagonal metal–organic frameworks with flexible ethoxy substituent†

Suvendu Sekhar Mondal,[a] Subarna Dey,[b] Igor A. Baburin,[c] Alexandra Kelling,[a] Uwe Schilde,[a] Gotthard Seifert,[c] Christoph Janiak[b] and Hans-Jürgen Holdt*[a]

A rare example of *in situ* linker generation with the formation of soft porous Zn- and Co-MOFs (IFP-9 and -10, respectively) is reported. The flexible ethoxy groups of IFP-9 and -10 protrude into the 1D hexagonal channels. The gas-sorption behavior of both materials for H_2, CO_2 and CH_4 showed wide hysteretic isotherms, typical for MOFs having a flexible substituent which can give rise to a gate effect.

Flexible or soft porous networks are known as third-generation porous coordination polymers that have gained much attention because of their interesting properties.[1–4] Compounds of this exclusive family of materials show a reversible dynamic response dependent on external stimuli, such as the presence/absence of specific guest molecules or even changes in temperature[5] and pressure.[6] As a result of this unique property, flexible MOFs have potential applications in selective gas adsorption/separation or chemical sensing.[3,7,8] Despite the fact that the number of responsive frameworks is still increasing, rational fine-tuning of the dynamic features of flexible MOFs has become more challenging.[3,9,10] The series of pillared-layered frameworks of the type $[M_2L_2P]_n$ (M = Co, Ni, Cu, Zn; L = dicarboxylate ligand; P = neutral pillar) were extensively studied in the past few years.[11–14] Due to the elastic paddlewheel building block, an intrinsic framework flexibility of these MOFs was observed.[11] Thus, the MOFs can exhibit slightly different crystal structures and cell volumes depending on the nature of the guest molecules adsorbed in the pores. In addition, reversible shrinkage and expansion of their unit cells (large pore → narrow pore → large pore) upon adsorption of alcohols was noticed for the reported MOFs.[15,16] In a related study, Fischer and coworkers have reported a series of MOFs by using a specifically functionalized bdc-type linker having dangling alkoxy substituents. Such frameworks exhibit a guest-dependent structural transformation and breathing effect.[17–19]

We have previously developed a new class of metal 2-substituted imidazolate-4-amide-5-imidate based metal–organic frameworks called IFP (Imidazolate Framework Potsdam).[20–22] The chelating 2-substituted imidazolate-4-amide-5-imidate ligands were generated *in situ* by partial hydrolysis of 2-substituted 4,5-dicyanoimidazole in the presence of a metal salt hydrate in *N*,*N*′-dimethylformamide (DMF) under solvothermal conditions, yielding IFP-1 to -4 and IFP-7.[20–22] Zinc-imidazolate-4-amide-5-imidate based IFP-7 showed gate effects due to its flexible methoxy substituent and selective CO_2 capture.[22] Herein, we report the syntheses of zinc and cobalt based imidazolate-4-amide-5-imidate frameworks called IFP-9 and -10, respectively, having a flexible ethoxy substituent. The gas sorption properties of IFP-9 and -10 again indicate flexible MOFs with a gate effect.

The MOFs $\{[Zn(L2)]\cdot 0.5DMF\}_n$ and $\{[Co(L2)]\cdot xH_2O\cdot yDMF\}_n$ (L2 = 2-ethoxyimidazolate-4-amide-5-imidate) are named IFP-9 and IFP-10, respectively. IFP-9 was synthesized by the reaction of 4,5-dicyano-2-ethoxyimidazole (L1) with an equimolar amount of $Zn(NO_3)_2\cdot 4H_2O$ in a mixture of DMF, ethanol and water under solvothermal conditions. The reaction conditions yielded *in situ* the 2-ethoxyimidazolate-4-amide-5-imidate linker (L2). Similarly, IFP-10 was formed by the reaction of L1 with an equimolar amount of $Co(NO_3)_2\cdot 6H_2O$ in DMF under solvothermal conditions (Scheme 1).

The degree of *in situ* hydrolysis of the cyano groups of 4,5-dicyano-2-ethoxyimidazolate (L1) into the corresponding imidazolate-4-amide-5-imidate linker (L2) was studied using infrared (IR) spectroscopy. The IR-spectra of the IFP-9 and IFP-10 manifested no stretching bands related to C≡N in

[a] *Institut für Chemie, Anorganische Chemie, Universität Potsdam, Karl-Liebknecht-Straße 24–25, 14476 Potsdam, Germany. E-mail: holdt@uni-potsdam.de; Fax: +49 331 977 5055; Tel: +49 331 977 5180*

[b] *Institut für Anorganische Chemie und Strukturchemie, Heinrich-Heine-Universität Düsseldorf, 40204 Düsseldorf, Germany. E-mail: janiak@uni-duesseldorf.de*

[c] *Institut für Physikalische Chemie und Elektrochemie, Technische Universität Dresden, 01062 Dresden, Germany*

† Electronic supplementary information (ESI) available: Detailed experimental procedure, IR spectra, PXRD patterns, TGA traces, table of X-ray data of IFP-9, gas adsorption data. CCDC 956082. For ESI and crystallographic data in CIF or other electronic format see DOI: 10.1039/c3ce41632a

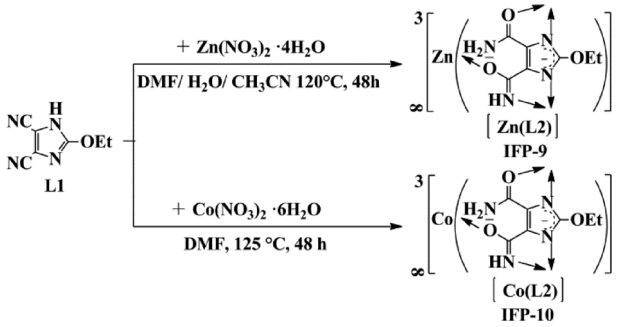

Scheme 1 Syntheses of IFP-9 and IFP-10.

the 2200–2230 cm^{-1} region. Instead, new typical bands for amide and imidate groups were observed at around 1560 cm^{-1} and 1660 cm^{-1}, respectively. Among other prominent IR changes, those associated with N–H resonances were noticeable. Centered at 3341 cm^{-1} (IFP-9) and 3335 cm^{-1} (IFP-10), a broad amide–imidate N–H band with a considerably fine structure was noted (Fig. S1, ESI†).

IFP-9 crystallizes in the highly symmetric rhombohedral space group $R\bar{3}$.[23] The asymmetric unit contains one Zn^{2+} ion and the bridging ligand L2 (Fig. S2, ESI†). The Zn^{2+} ion is pentacoordinated by the donor atoms of three L2 ligands to form a distorted environment with a trigonal-bipyramidal geometry (Fig. 1). In turn, L2 acts as pentadentate linker that coordinates three Zn^{2+} ions. This means that Zn^{2+} ions and bridging L2 ligands act as 3-connected topological species forming a net with a rare uninodal topology, named *etb*.[20,24,25] The topology of IFP-9 is classified by the vertex symbol 3.6.10.15.

In this arrangement, imidates N3 and O2 and the amide O3 reside in equatorial positions and two imidazolate N atoms (N1 and N2) occupy the axial positions (Fig. 1). This five-fold coordination leads to a Zn^{2+} centre with Lewis acid properties.

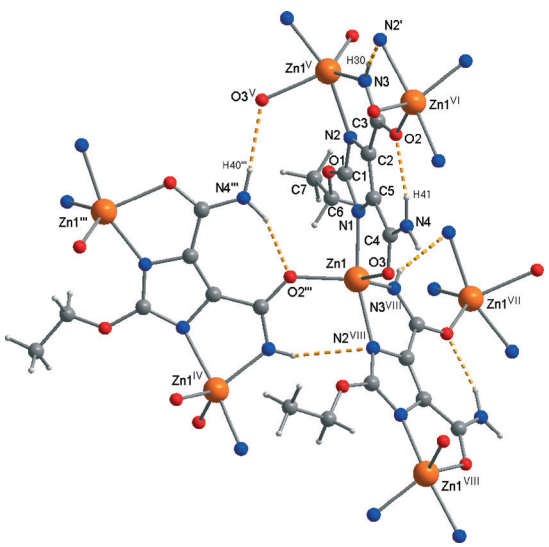

Fig. 1 Section of the crystal structure of IFP-9, showing the coordination environment of Zn^{2+}, the bridging mode of the linker L2 and the hydrogen bonds (dotted lines). For the symmetry codes and details of hydrogen bonds, see the ESI.†

The amide and imidate groups are formed by the *in situ* partial hydrolysis of cyano groups and enable each L2 ligand to participate in the formation of two five-membered chelate rings. One ring forms by coordinating a Zn^{2+} ion to the N1 (imidazolate) atom and the O3 (amide) atom. The other chelate ring forms by coordinating a second Zn^{2+} ion to the N2 (imidazolate) atom and the N3 (imidate) atom. The negatively charged O2 (imidate) atom is coordinated to a third Zn^{2+} ion.

The structure of IFP-9 is further stabilized by three hydrogen bonds (Fig. 1), one intramolecular bond between a nitrogen atom of an amide group and an imidate O atom (N4–H41···O2) and intermolecular hydrogen bonds between an imidate NH group and an imidazolate N atom (N3–H30···N2), as well as between a nitrogen atom and an oxygen atom of the amide groups (N4–H40···O3). The hydrogen-bonding parameters as well as the symmetry operators are listed in Table S4 in the ESI.† The structure of IFP-9 possesses 1D hexagonal channels running along 0, 0, *z*; 1/3, 2/3, *z*; and 2/3, 1/3, *z* (Fig. 2).

The walls of the hexagonal channel in IFP-9 are essentially constructed by the rigid and planar imidazolate-amide-imidate linker L2. The Zn^{2+} ions are located almost on the edges of the hexagonal channels. They are bridged by the L2 linkers through coordination with both N imidazolate atoms. The amide and imidate functional groups of the bridging ligand L2 are embedded in the wall of the channel. The imidate group bridges two Zn^{2+} ions of two channel edges through its N and O atoms. The three different types of hydrogen bonds are all confined to the channel wall as well. The localization of the amide and imidate groups and the hydrogen bonds in the channel walls, and of the pentacoordinated Zn^{2+} ions at the edges of the hexagonal channels, as well as the ethoxy substituents which point into the channels, polarizes and functionalizes the coordination space of this MOF.

Moreover, after several attempts, we could not find a suitable crystal of IFP-10 for single crystal X-ray measurement. Hence, the structural model of IFP-10 was constructed by using the single-crystal X-ray refinement of IFP-1[20] which was further optimized by using an *ab initio* density functional theory (DFT) method. The PXRD pattern of the optimized IFP-10 structure is in good agreement with the experimental data (Fig. 3). The theoretically optimized structure of IFP-10 also possesses 1D hexagonal channels (Fig. 2b). The ethoxy groups protrude into the open channels and determine their pore aperture. The ethyl group of the ethoxy moiety is disordered over two equally occupied sites. By considering the van der Waals radii, the pore aperture diameter of the channels in IFP-9 was estimated as 0.60 and 0.35 Å for the corresponding disordered species. For IFP-10, a diameter of 0.30 Å was calculated from the theoretically estimated structure. The void spaces in IFP-9 and IFP-10 represent 23% and 26%, respectively. For the void calculation, the PLATON toolkit was used.[26,27]

Thermogravimetric analysis (TGA) for as-synthesized IFP-9 indicated a gradual weight-loss of about 5% starting from 200 °C up to 325 °C which corresponds to partial loss of DMF guest species, followed by framework decomposition above 325 °C. As-synthesized IFP-10 showed a negligible weight-loss

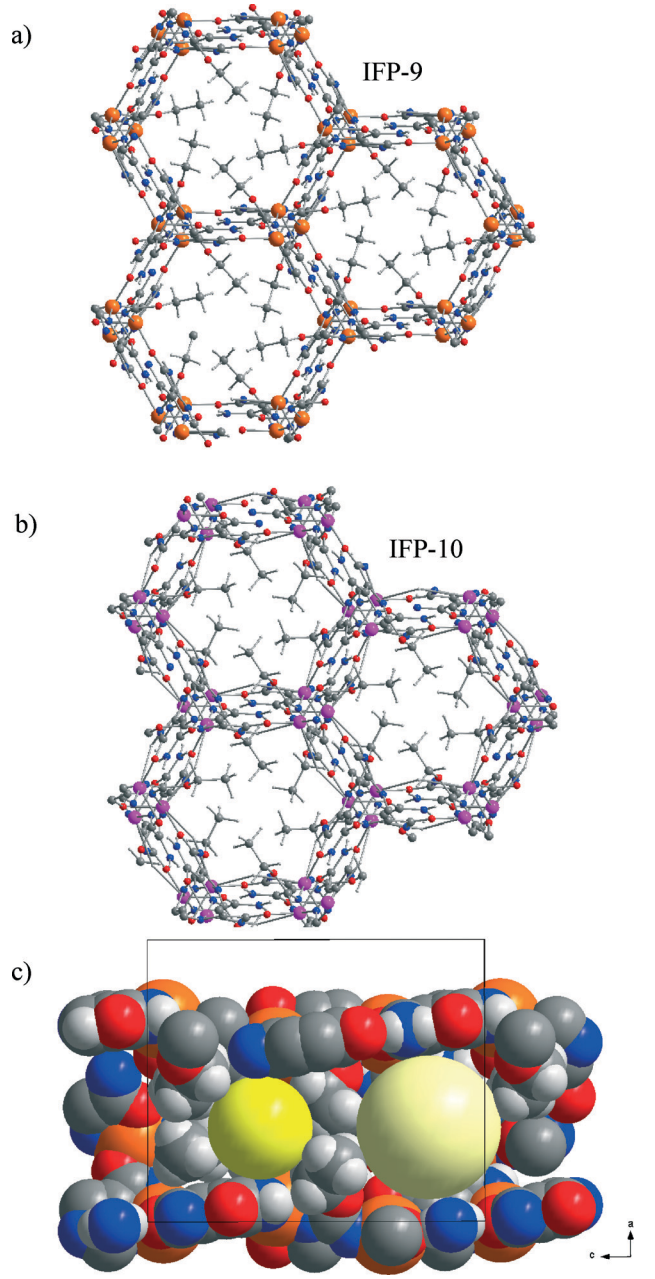

Fig. 2 Hexagonal channels with different accessible diameters – a) for IFP-9 (Zn-centre), b) for IFP-10 (Co-centre); orange – Zn, pink – Co, blue – N, red – O, dark gray – C, light gray – H; the ethyl group in IFP-9 is disordered; only one species is drawn. The structure of IFP-10 is based on *ab initio* density functional calculations. (c) Insight into one channel of IFP-9 (running along c) with two different void volumes – for details, see the squeeze output at the end of the cif.

step of 5% at 25–225 °C, corresponding to the release of solvent molecules (Fig. S3, ESI†). TGA traces show that after solvent removal, both IFPs are stable up to 300 °C. Materials were activated at 200 °C at 10^{-3} mbar pressure for 24 h. Powder X-ray diffraction patterns (PXRD) of activated samples exhibited sharp diffraction peaks similar to the as-synthesized samples (Fig. 3). Thus, the porous frameworks maintained crystalline integrity even without solvent molecules.

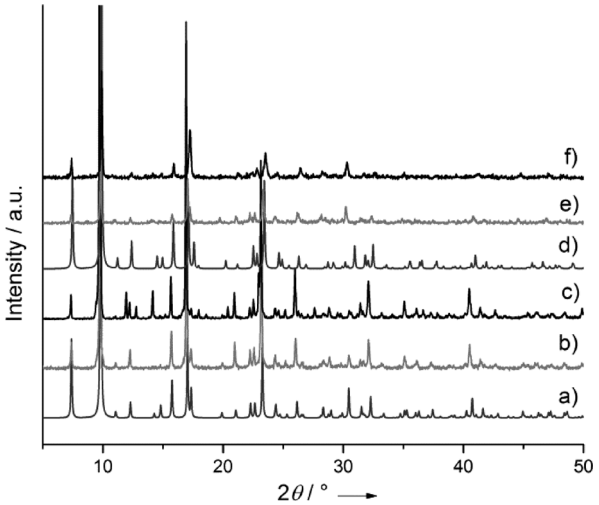

Fig. 3 Powder X-ray diffraction patterns of IFP-9; a) simulated, b) as-synthesized and c) activated, and of IFP-10; d) simulated, e) as-synthesized and f) activated.

Activated IFP-9 and -10 are expected to show gas-sorption selectivity towards small polar molecules due to their polar and flexible ethoxy side chains. The gas sorption isotherms of N_2, H_2, CH_4, and CO_2 for IFP-9 are recorded at various temperatures up to 1 bar (Fig. 4 and 5). IFP-9 and -10 barely adsorbed N_2 at 77 K, which can be attributed to a narrow pore size of the channels (0.60 and 0.35 Å for IFP-9 and 0.30 Å for IFP-10). Hence, N_2 molecules (kinetic diameter of 3.64 Å) cannot diffuse into the small channels. From the estimated Brunauer–Emmett–Teller (BET) surface area for IFP-9 and -10 of 7 and 13 $m^2\ g^{-1}$, respectively, it can be concluded that N_2 is adsorbed at the outer surface only. The CO_2, CH_4 and H_2 sorption isotherms show very different sorption behaviors. The low-pressure CO_2 sorption measurements for IFP-9 (at 273 K, Fig. 4a) and IFP-10 (at 273 K and 298 K, Fig. 5a) indicate CO_2 uptake with a broad hysteresis for the desorption branch. Such hysteretic behavior was also observed for flexible MOFs like IFP-7 and other MOFs having flexible substituents.[17–19,22] The uptake of CO_2 by IFP-9 and IFP-10 at 273 K and 1 bar is 5 $cm^3\ g^{-1}$ and 39 $cm^3\ g^{-1}$, respectively. Because of the small-pore aperture windows (see above), the CO_2 molecules are preferably located in cavities ("zero-dimensional closed space").[28] Notably, IFP-9 and IFP-10 also adsorb 2.5 $cm^3\ g^{-1}$ and 6 $cm^3\ g^{-1}$ CH_4 at 273 K and 1 bar, respectively, despite their narrow pore apertures (Fig. 4a for IFP-9 and Fig. 5b for IFP-10). Also, H_2 is adsorbed at 77 K up to 8.8 and 5.2 $cm^3\ g^{-1}$ in IFP-9 and -10, respectively, at 1 bar (Fig. 4b for IFP-9 and Fig. 5b for IFP-10).

The reason that N_2 at 77 K is not adsorbed presumably because of activated diffusion effects associated with the low thermal energy of the adsorbate relative to the high barrier for diffusion through the small-pore aperture windows.[29] In other words, at slow thermal motion at 77 K, the N_2 molecule will statistically only seldom approach the small-pore aperture with the correct orientation for penetration, that is, in line with its molecule axis. While H_2 and CO_2 are adsorbed at 77 K and 273 K, respectively, N_2 is not adsorbed at 77 K,

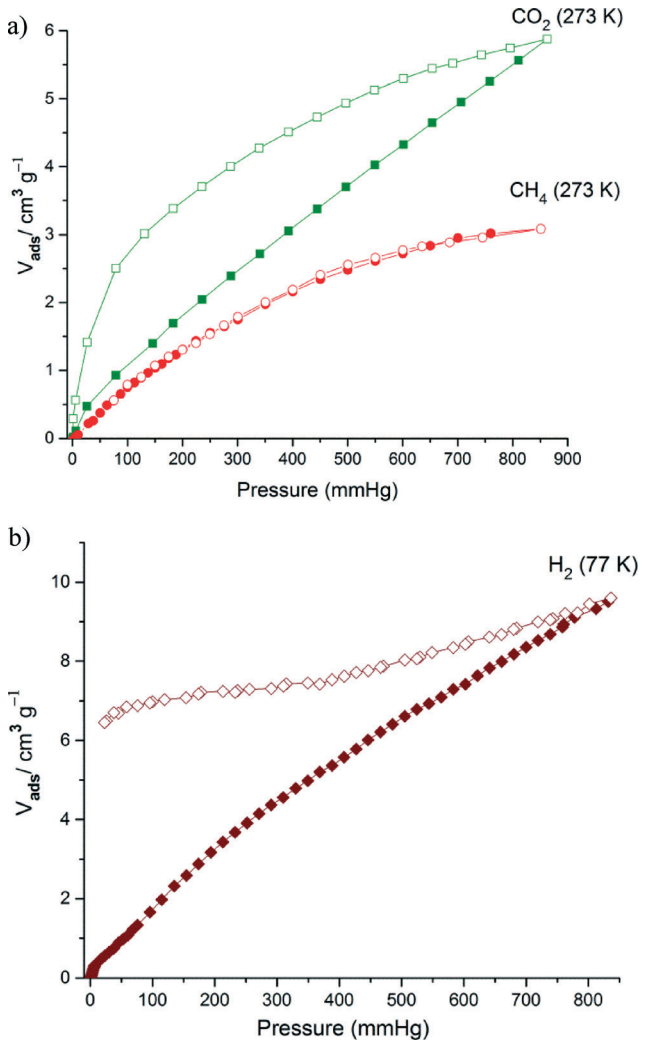

Fig. 4 Gas sorption isotherms for activated IFP-9. Adsorption and desorption branches are indicated by closed and open symbols, respectively.

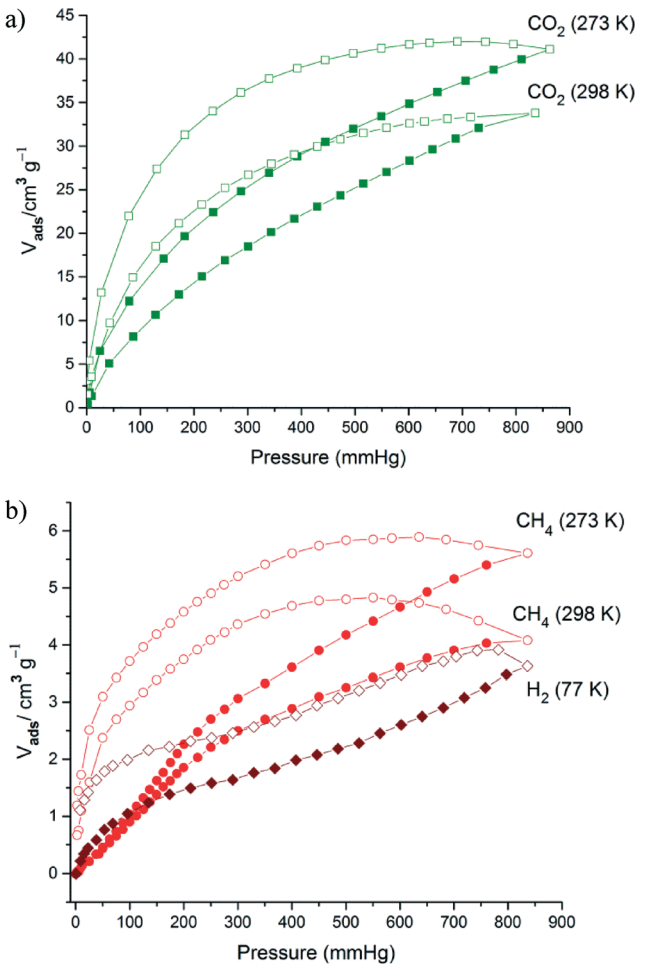

Fig. 5 Gas sorption isotherms for activated IFP-10. Adsorption and desorption branches are indicated by closed and open symbols, respectively.

which is a frequently encountered phenomenon characterized by the kinetic hindrance of small pores or pore aperture windows.[30] It is suggested that the passage of guest molecules through the small-pore aperture windows in and out of the cavities proceeds through a temporary expansion of the window size. The desorption branches of CH_4 isotherms for IFP-10 show a wide desorption hysteresis. The CH_4 sorption behavior of IFP-10 can be attributed to a kinetic trap created by the polar flexible ethoxy substituent and imidazolate-amide-imidate channel walls, acting as a gate that regulates the access and release of CH_4 into and from the channels. Such broad desorption behaviour for the CH_4 isotherm at atmospheric pressure is rarely observed in microporous MOFs.[22,31] Another way to prove the flexibility of the frameworks is by H_2 sorption. Although IFPs adsorb a low amount of H_2 at atmospheric pressure, they show a wide desorption hysteresis. As already mentioned, IFP-9 possesses pore aperture windows of 0.35 Å to the solvent-depleted cavities of 8.0 and 5.8 Å diameter (see Fig. 2c), and ethoxy groups from the ligand form the pore aperture windows. Incoming gas molecules have to widen the windows by changing the conformation of the ethoxy groups arranged on the C2-atom of the imidazole ring. Because of the lower kinetic diameter of CO_2 (3.3 Å), in comparison to that of CH_4 (3.8 Å), the twist of the ethyl groups for incoming CO_2 has to be smaller as it has to be for CH_4. Moreover, this behavior demonstrates that the selective uptake for CO_2 over N_2, CH_4 and H_2 could be attributed to the difference in polarizability of adsorbate molecules (average electric dipole polarizabilities: CO_2 2.911 × 10^{-24} cm^3, N_2 1.7403 × 10^{-24} cm^3, CH_4 2.593 × 10^{-24} cm^3).[32] The interactions are expected between the polar functional groups (amide and imidate) and CO_2, which has a significant quadrupole moment, while CH_4 has none. Therefore, IFP-10 also shows a higher CO_2 uptake compared to IFP-9 due to the presence of an unsaturated metal site of the paramagnetic Co centre (d^7-system). The Zn centre has the electronic state d^{10} and is a diamagnetic system. We anticipated that the Co centres in IFP-10 have a higher potential to polarize CO_2 molecules than the Zn-based IFP-9. This behaviour was also previously observed for the Co-based isostructural IFP-5.[33] A similar wide hysteretic H_2 uptake was observed by a nanoporous octanuclear Cu^{2+} structure and its Co^{2+} ion-exchanged material.[34]

In conclusion, we report an *in situ* formed 2-ethoxyimidazolate-4-amide-5-imidate linker with its isostructural MOFs IFP-9 and-10. Porous 3D frameworks with 1D hexagonal channels with pore aperture diameters of 0.35 Å and 0.30 Å are formed for IFP-9 (Zn) and IFP-10 (Co), respectively. The structure of IFP-9 was determined by X-ray crystallographic analysis. The structure of IFP-10 was determined by a combination of PXRD and structure modelling and was confirmed by IR spectroscopy. Due to the polar ethoxy group and narrow pore apertures, wide hysteretic isotherms for H_2, CO_2 and CH_4 were observed. The very broad desorption hysteretic behaviour of CH_4 uptake for IFP-10 is not commonly observed for microporous MOFs. Such gas-sorption behaviour is typical for the MOFs having flexible substituents. Due to the narrow pore apertures with flexible ethoxy groups, IFP-9 and -10 could be useful for potential gas mixture separation in comparison with other IFP materials at high pressure measurements. Moreover, research to extend this approach to other transition metal ions and other flexible substituent-based IFPs is in progress.

Acknowledgements

This work is financially supported by Priority Program 1362 of the German Research Foundation on "Metal–Organic Frameworks." We thank Dr. C. Günter (Institut für Erd- und Umweltwissenschaften, Universität Potsdam, Germany) for powder X-ray diffraction measurements.

Notes and references

1 S. Kitagawa and K. Uemura, *Chem. Soc. Rev.*, 2005, **34**, 109–119.
2 G. Férey and C. Serre, *Chem. Soc. Rev.*, 2009, **38**, 1380–1399.
3 (*a*) S. Horike, S. Shimomura and S. Kitagawa, *Nat. Chem.*, 2009, **1**, 695–704; (*b*) K. Sumida, D. L. Rogow, J. A. Mason, T. M. McDonald, E. D. Bloch, Z. R. Herm, T. H. Bae and J. R. Long, *Chem. Rev.*, 2012, **112**, 724–781.
4 R. Kitaura, K. Seki, G. Akiyama and S. Kitagawa, *Angew. Chem., Int. Ed.*, 2003, **42**, 428–431.
5 Y. Liu, J. Her, A. Dailly, A. J. Ramirez-Cuesta, D. A. Neumann and C. M. Brown, *J. Am. Chem. Soc.*, 2008, **130**, 11813–11818.
6 P. G. Yot, Q. Ma, J. Haines, Q. Yang, A. Ghoufi, T. Devic, C. Serre, V. Dmitriev, G. Férey, C. Zhong and G. Maurin, *Chem. Sci.*, 2012, **3**, 1100–1104.
7 J.-R. Li, J. Sculley and H.-C. Zhou, *Chem. Rev.*, 2012, **112**, 869–932.
8 L. E. Kreno, K. Leong, O. K. Farha, M. Allendorf, R. P. Van Duyne and J. T. Hupp, *Chem. Rev.*, 2012, **112**, 1105–1125.
9 P. Horcajada, F. Salles, S. Wuttke, T. Devic, D. Heurtaux, G. Maurin, A. Vimont, M. Daturi, O. David, E. Magnier, N. Stock, Y. Filinchuk, D. Popov, C. Riekel, G. Férey and C. Serre, *J. Am. Chem. Soc.*, 2011, **133**, 17839–17847.
10 T. Lescouet, E. Kockrick, G. Bergeret, M. Pera-Titus, S. Aguado and D. Farrusseng, *J. Mater. Chem.*, 2012, **22**, 10287–10293.
11 D. N. Dybtsev, H. Chun and K. Kim, *Angew. Chem., Int. Ed.*, 2004, **43**, 5033–5036.
12 K. L. Mulfort and J. T. Hupp, *J. Am. Chem. Soc.*, 2007, **129**, 9604–9605.
13 N. Yanai, T. Uemura, M. Inoue, R. Matsuda, T. Fukushima, M. Tsujimoto, S. Isoda and S. Kitagawa, *J. Am. Chem. Soc.*, 2012, **134**, 4501–4504.
14 H. C. Hoffmann, B. Assfour, F. Epperlein, N. Klein, S. Paasch, I. Senkovska, S. Kaskel, G. Seifert and E. Brunner, *J. Am. Chem. Soc.*, 2011, **133**, 8681–8690.
15 K. Uemura, Y. Yamasaki, F. Onishi, H. Kita and M. Ebihara, *Inorg. Chem.*, 2010, **49**, 10133–10143.
16 J. S. Grosch and F. Paesani, *J. Am. Chem. Soc.*, 2012, **134**, 4207–4215.
17 S. Henke, R. Schmid, J.-D. Grunwaldt and R. A. Fischer, *Chem.–Eur. J.*, 2010, **16**, 14296–14306.
18 S. Henke, A. Schneemann, A. Wütscher and R. A. Fischer, *J. Am. Chem. Soc.*, 2012, **134**, 9464–9474.
19 S. Henke and R. A. Fischer, *J. Am. Chem. Soc.*, 2011, **133**, 2064–2067.
20 F. Debatin, A. Thomas, A. Kelling, N. Hedin, Z. Bacsik, I. Senkovska, S. Kaskel, M. Junginger, H. Müller, U. Schilde, C. Jäger, A. Friedrich and H.-J. Holdt, *Angew. Chem., Int. Ed.*, 2010, **49**, 1258–1262.
21 F. Debatin, K. Behrens, J. Weber, I. A. Baburin, A. Thomas, J. Schmidt, I. Senkovska, S. Kaskel, A. Kelling, N. Hedin, Z. Bacsik, S. Leoni, G. Seifert, C. Jäger, C. Günter, U. Schilde, A. Friedrich and H.-J. Holdt, *Chem.–Eur. J.*, 2012, **18**, 11630–11640.
22 S. S. Mondal, A. Bhunia, I. A. Baburin, C. Jäger, A. Kelling, U. Schilde, G. Seifert, C. Janiak and H.-J. Holdt, *Chem. Commun.*, 2013, **49**, 7599–7601.
23 Crystal data for IFP-9: $C_{8.5}H_{11.5}N_{4.5}O_{3.5}Zn$, M_r = 298.09 g mol^{-1}, crystal dimensions 0.30 × 0.21 × 0.12 mm, trigonal, space group $R\bar{3}$, $a = b$ = 18.0166(5), c = 18.6077(5) Å, V = 5230.8(2) Å^3, Z = 18, ρ_{calcd} = 1.70 g cm^{-1}; $\mu(Mo_{K\alpha})$ = 2.12 mm^{-1}, T = 210 K, $2\theta_{max}$ = 55.0°, 29 403 reflections measured, 2681 unique (R_{int} = 0.0211), R = 0.0212, wR = 0.0559 ($I > 2\sigma(I)$). For details of the data collection and the structure solution and refinement see ESI.† CCDC 956082 contains the supplementary crystallographic data for this paper. These data can be obtained free of charge from the Cambridge Crystallographic Data Centre *via* www.ccdc.cam.ac.uk/data_request/cif.
24 N. L. Rosi, J. Kim, M. Eddaoudi, B. Chen, M. O'Keeffe and O. M. Yaghi, *J. Am. Chem. Soc.*, 2005, **127**, 1504–1518.
25 O.-R. Fang, G.-S. Zhu, Z. Jin, Y.-Y. Ji, J.-W. Ye, M. Xue, H. Yang, Y. Wang and S.-L. Qui, *Angew. Chem., Int. Ed.*, 2007, **46**, 6638–6642.
26 A. Bondi, *J. Phys. Chem.*, 1964, **68**, 441–451.
27 A. L. Spek, *PLATON: A Multipurpose Crystallographic Tool*, Utrecht University, Utrecht, The Netherlands, 2001.
28 S.-I. Noro, S. Kitagawa, T. Akutagawa and T. Nakamura, *Prog. Polym. Sci.*, 2009, **34**, 240–279.
29 A. J. Fletcher, E. J. Cussen, T. J. Prior, M. J. Rosseinsky, C. J. Kepert and K. M. Thomas, *J. Am. Chem. Soc.*, 2001, **123**, 10001–10011.
30 (*a*) C. Janiak, *Chem. Commun.*, 2013, **49**, 6933–6937; (*b*) C. Heering, I. Boldog, V. Vasylyeva, J. Sanchiz and C. Janiak, *CrystEngComm*, 2013, DOI: 10.1039/C3CE41426D, in press.

31 D. Zhao, D. Yuan, R. Krishna, J. M. van Baten and H.-C. Zhou, *Chem. Commun.*, 2010, **46**, 7352–7354.
32 D. R. Lide, *CRC Handbook of Chemistry and Physics*, CRC Press, Boca Raton, FL, 2009, Table 4, pp. 10–196.
33 F. Debatin, J. Möllmer, S. S. Mondal, K. Behrens, A. Möller, R. Staudt, A. Thomas and H.-J. Holdt, *J. Mater. Chem.*, 2012, **22**, 10221–10227.
34 J. Zhao, L. Mi, J. Hu, H. Hou and Y. Fan, *J. Am. Chem. Soc.*, 2008, **130**, 15222–15223.